China Instrument and Control Society
Instrumentation

OPEN ACCESS

INSTRUMENTATION, Vol. 12, No. 1, March 2025 https://doi.org/10.15878/j.instr.202400215

Article

Analysis of Interactions Between Vibration Modes of Piezoelectric Vibrators

Chong Li[1*], Cunyue Lu[2]

[1] School of Intelligent Manufacturing and Control Engineering, Shanghai Polytechnic University, Shanghai 201209, China

[2] School of Sensing Science and Engineering, Shanghai Jiao Tong University, Shanghai 200240, China

[*] Corresponding author email: uestc2007@yeah.net

Abstract: To broaden the frequency regulation range of piezoelectric motors, this paper proposes a piezoelectric vibrator that operates in multiple in-plane vibration modes with distinct resonance frequencies. The piezoelectric vibrator was constructed by reasonably arranging multiple groups of piezoelectric ceramic (PZT) sheets based on the most typical rectangular plate piezoelectric motors. Suitable working modes were selected, and the excitation method of these operating modes was also analyzed. Besides, interactions between selected operating modes were also investigated. The finite element software, ANSYS, was adopted to optimize the structural parameters of the vibrator through modal analysis to match the resonance frequencies of specific modes. After that, whether the selected operating modes can be successfully motivated was verified by harmonic response analysis. Finally, the vibration characteristics of piezoelectric vibrators under conventional vibration modes and multiple modes were acquired by transient analysis, respectively. Simulation results reveal that under dual-frequency excitation scheme 1, response displacements of the driving point are relatively larger. This strategy not only facilitates the excitation of B_4 mode but also enables control over the ratio of horizontal to vertical displacements of the driving point. Additionally, incorporating B_4 mode expands the frequency adjustment range of piezoelectric vibrators.

Keywords: piezoelectric vibrator; mode; interaction; PZT; finite element; vibration characteristics

Citation: Chong Li, Cunyue Lu. "Analysis of Interactions Between Vibration Modes of Piezoelectric Vibrators." Instrumentation 12, no. 1 (March 2025). https://doi.org/10.15878/j.instr.202400215

1 Introduction

Piezoelectric motors utilize the inverse piezoelectric effect of piezoelectric materials. By mechanically amplifying the microscopic deformation of piezoelectric materials through resonance and friction coupling, the macroscopic rotation of the rotor can be achieved[1-3]. Compared to electromagnetic motors, piezoelectric motors possess individual advantages such as no electromagnetic interference, high positioning accuracy and power density. Currently, piezoelectric motors have found widespread applications in displacement platforms, surgical robots, and precision optical equipment[4-6].

Piezoelectric motors are primarily classified into traveling wave type and standing wave type. Among them, the traveling wave motors are currently the most commonly used and mainly consist of the piezoelectric stator (vibrator), rotor, and preloading mechanism. As the core component of piezoelectric motors, piezoelectric vibrators typically require a set of working modes with identical resonance frequencies and a 90-degree phase difference. By applying sinusoidal excitation signals with a frequency equal to the resonance frequency of working modes[7-9] and a phase difference of 90-degree to piezoelectric ceramics (PZT), two working modes can be simultaneously excited[10,11]. Then, a superposed traveling wave is generated. Typically, the mechanical performances of piezoelectric motors can only be adjusted by the amplitude, frequency, and phase difference of driving voltages[2]. The amplitude adjustment range has a large dead zone. The phase difference adjustment is not suitable for single-phase piezoelectric motors and may alter the motion trajectory of stator driving particles[2, 12], affecting motor performance and complicating the drive circuit. The frequency adjustment is the most commonly used method, as it offers a quick response and facilitates low-speed starting. However, once the motor structure, the arrangement, and polarization direction of PZTs are determined during the design process, working modes and their resonance frequency are normally fixed. Additionally, piezoelectric motors typically operate in a resonant state at ultrasonic frequencies, and their performance is highly sensitive to frequency changes, with even slight variations in frequency causing significant changes in rotation speed. Due to the fixed working modes of piezoelectric motors, the frequency tuning range is narrow and frequency modulation accuracy is limited[13].

To broaden the frequency regulation range of piezoelectric motors, researchers have carried out a lot of studies on multi-mode piezoelectric motors. The author has proposed a bar-shaped piezoelectric motor with multiple working modes, and analyzed interactions between all the selected vibration modes[13]. In order to further expand the study of multi-mode piezoelectric motors, this paper investigates vibration characteristics and motion trajectory of rectangular plate piezoelectric motors in a variety of multi-mode excitation through the finite element analysis software ANSYS. Interactions between these working modes are also explored. This paper helps to promote the research and development of multi-mode piezoelectric motors. Fig. 1 gives the overall design flow chart.

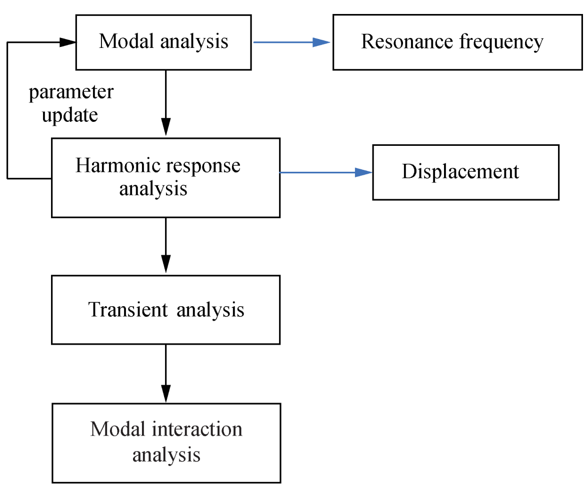

Fig.1 Overall design flow chart

2 Structure and Excitation

The constructed rectangular plate piezoelectric vibrator is shown in Fig. 2, consisting of a metal body with a through hole in the middle and two groups of PZTs symmetrically pasted on and below the metal body. The polarization of the top PZTs (P_1 to P_8) is positive along the z axis, while the bottom PZT (P_9 to P_{16}) is negative along the z axis.

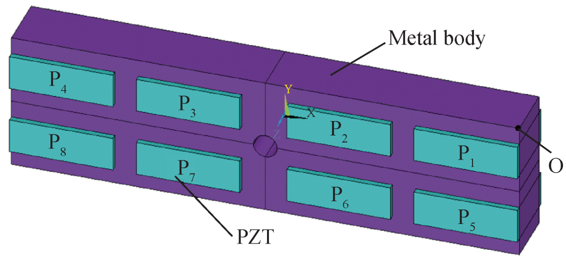

Fig.2 Structure diagram of piezoelectric vibrator

The selected working modes which are the first-order longitudinal vibration mode (L_1), the second-order bending mode (B_2) and the fourth-order bending mode (B_4), are all shown in Fig. 3. Among them, L_1 and B_2 are the working modes of conventional rectangular plate piezoelectric motors. The common node of L_1 and B_2 modes is located at the center of the rectangular plate and is usually set as the tightening point. To ensure the in-plane vibration characteristic of rectangular plate piezoelectric motors and minimize the vibration displacement at the clamping point, thereby minimizing the frequency shift caused by mechanical clamping, the B_4 mode is added to the working modes.

To analyze the excitation way of operating modes, the vibration curves of three modes are plotted on the

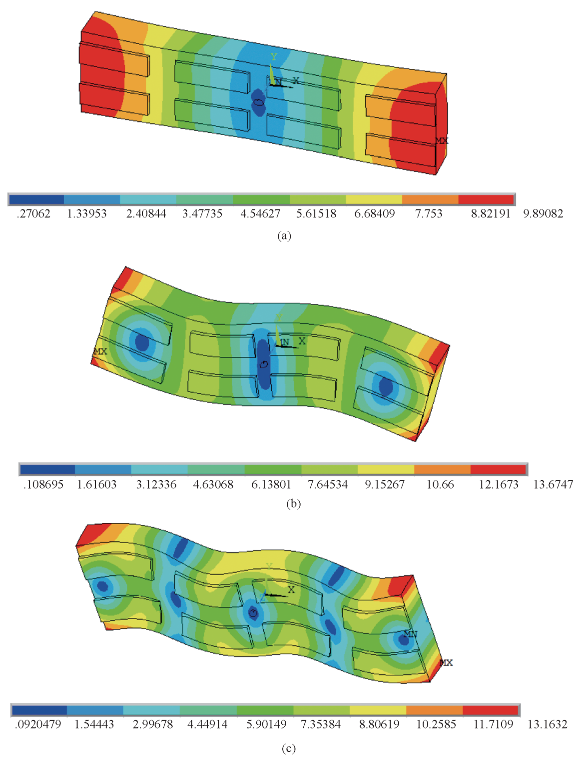

Fig.3 Vibration modes: (a) L_1; (b) B_2; (c) B_4

same coordinate system, as shown in Fig. 4. The dashed rectangular boundary represents the entire PZT plate. The x-axis represents the distribution of particles and the y-axis stands for the vibration of particles. For the L_1 mode, particles at both sides of the x-axis vibrate in opposite directions. Therefore, the PZT plate needs to be divided into left and right parts, and the phase difference of excitation voltages between the two parts is 180 degrees. For the B_2 mode, to form a bending vibration on the right side of the y-axis, PZT plate on the right side of the y-axis needs to be divided into upper and lower parts, with the upper part elongating and the lower part contracting. Similarly, to form a bending vibration on the left side of the y-axis, PZT plate on the left side of the y-axis also needs to be divided into upper and lower parts, but the upper part contracts and the lower part elongates. The B_4 mode is a higher-order mode of B_2, and their vibrations are similar. Based on the analysis of B_2 mode, to excite the B_4 mode, PZT plate needs to be divided into eight parts, as shown in Fig. 4.

To increase the vibration displacement of particles and deduce interactions between different modes by comparing the vibration characteristics of the particles, eight PZTs are also symmetrically pasted onto the bottom of the metal body, resulting in the piezoelectric vibrator structure shown in Fig. 4. Table 1 lists the excitation voltage signals that need to be applied to PZTs (P_1 to P_8) to excite the vibration modes. Since the polarization directions of bottom PZTs and top PZTs are opposite, the excitation signals applied to them are exactly the same. In addition, because L_1 and B_2 modes are the working modes of conventional rectangular plate in-plane piezoelectric motors, their excitation ways are combined in Table 1. In Table 1, sin and cos respectively represent applying sinusoidal and cosine excitation signals to the corresponding PZTs.

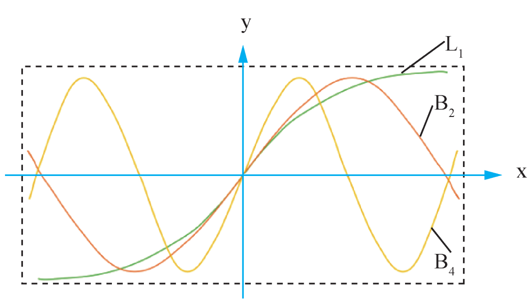

Fig.4 Vibration curves of the three operating modes

Table 1 Excitation signals applied to PZTs

Mode	P_1	P_2	P_3	P_4	P_5	P_6	P_7	P_8
L_1 and B_2	sin	sin	cos	cos	cos	cos	sin	sin
B_4	cos	sin	cos	sin	sin	cos	sin	cos

3 Simulation

A finite element model of the piezoelectric vibrator was constructed using ANSYS software, with the parameters of the metal body and PZTs referenced from [10]. Initially, the resonance frequencies of the working modes were adjusted through modal analysis. By adjusting the structural parameters of the piezoelectric vibrator (length, wideness, thickness of the metal body and PZTs; pasting position of PZTs; the dimension of through hole), the resonance frequencies of L_1 and B_2 modes should be brought closer, and there is no other interfering modes near L_1, B_2, and B_4 modes. After multiple simulation calculations, the resonance frequencies of L_1, B_2, and B_4 modes are 38.216 kHz, 38.263 kHz, and 79.055 kHz, respectively, with a frequency difference of 47 Hz between L_1 and B_2 modes, meeting actual application requirements. The corresponding length, width, and thickness of the metal body are 43 mm, 12 mm, and 5 mm, respectively, with a radius of 1 mm for the central hole. The length, width, and thickness of PZTs are 8.75 mm, 3 mm, and 0.5 mm, respectively, with a horizontal distance of 2 mm between P_2 and P_1 and a vertical distance of 1.5 mm from the top surface of the metal body.

Given the distinct excitation methods for B_2 and B_4 modes, three different excitation schemes were employed in harmonic response analysis. For excitation way 1, all the PZTs are supplied with the same driving signals of B_4. For excitation way 3, all the PZTs are supplied with the same driving signals of B_2. For excitation way 2, different electric signals of B_2 and B_4 are respectively applied to the PZT plates pasted above and below the metal body.

Firstly, the harmonic response results under excitation scheme 1 were analyzed. The amplitude of excitation voltage is 200 V. A critical issue in harmonic response analysis is the determination of structural damping. After comprehensive analysis, Rayleigh damping was adopted in this study. The Alpha and Beta damping coefficients, α_z and β_z, are used to define Rayleigh damping, and they are usually derived from the structural damping ratio ε_z. In practical applications, α_z is zero. Then, the relationship between β_z and ε_z is expressed as

$$\beta_z = 2\varepsilon_z/\omega_i \tag{1}$$

where ω_i is the angular frequency of excitation signals. The structural damping ratio is set to be 0.3%. To accurately observe the resonance of L_1 and B_2 modes, the frequency sweep range is initially set from 36 kHz to 39 kHz, with 50 substeps. ω_i is 38.24 kHz. Assuming that point o in Fig. 1 is selected as the observation point, the maximum response displacements of the particle in horizontal and vertical directions respectively correspond to resonance frequencies of 38.214 kHz and 38.250 kHz, which also refer to the resonant frequencies of L_1 and B_2 modes, indicating that both modes were successfully excited. The slight deviation of the resonant frequencies obtained from harmonic response analysis compared to modal analysis is primarily attributed to the applied excitation voltage.

To further verify whether B_4 mode can be excited under this excitation scheme, the frequency sweep range is extended to 80 kHz, and the number of sub-steps is increased to 500. Due to the wide frequency sweep range and the strong frequency dependence of Beta damping, only the damping ratio is used for broadband harmonic response analysis. The calculated frequency response curve of the particle is shown in Fig. 5.

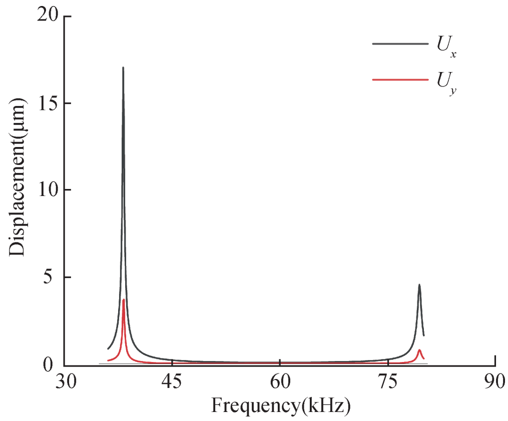

Fig.5 Displacement frequency curve of the point o under excitation way 1

Fig. 5 shows that, except for the working modes L_1, B_2, and B_4, no interference modes are excited. Due to the wide frequency sweep range and the small frequency difference between L_1 and B_2 modes, the displacement response curves in Fig. 5 cannot accurately distinguish these two resonance modes. B_4 mode corresponds to the second resonance peak, with a resonance frequency of 79 kHz.

Subsequently, displacement response characteristics of the point were calculated under excitation schemes 2 and 3, respectively. The results are generally similar to those under excitation scheme 1, but a small number of interference modes are excited under excitation scheme 2, leading to a decrease in the displacement corresponding to B_4 mode. Table 2 presents the results of harmonic response analysis under three excitation ways. The results in Table 2 show that all three excitation schemes can excite L_1, B_2, and B_4 modes. Under excitation scheme 1, the response displacement under resonance 2 (B_4 mode) is the largest, while under excitation scheme 3, the response displacement under resonance 1 (L_1 and B_2 modes) reaches the largest. Although excitation scheme 2 helps to increase the response displacement under resonance 1, it reduces the response displacement under resonance 2. Under excitation scheme 3, the response displacement under resonance 2 is slightly higher compared to excitation scheme 2. The reason may be that when different excitation voltages are applied to PZTs bonded to the upper and lower surfaces of the metal body, the response displacement of B_4 mode is significantly suppressed. Moreover, the excitation way of B_2 mode can only excite a small amount of displacement under B_4 mode. Based on the results in Table 2, it can only be derived that three excitation schemes have different effects on response displacements under two resonance states, but the effect on steady-state displacement of particles under combined action of operating modes cannot be obtained. Moreover, it does not conform to the actual operating states of vibrators. The frequency of excitation voltages applied to PZTs bonded to the upper and lower surfaces of the metal body during the frequency sweep of harmonic response analysis is the same.

Table 2 Harmonic response displacement of the point under three excitation methods

	Resonance 1 (μm)		Resonance 2 (μm)	
	U_x	U_y	U_x	U_y
Excitation 1	17	3.7	4.6	0.8
Excitation 2	19	7.2	1.5	0.3
Excitation 3	21.5	10.8	1.6	0.4

To further analyze the impact of three excitation schemes on actual operating states of displacement and to verify interactions between different working modes, transient analysis was also conducted. To excite L_1 and B_2 modes, excitation signals with a frequency of 38.2 kHz were applied. To actuate B_4 mode, the frequency of excitation signals was set to be 79 kHz. To distinguish driving voltages with different frequencies, they were applied separately to PZTs bonded to the upper and lower surfaces of the metal body. In transient analysis, the amplitude of excitation voltages was also set to be 200 V, and 40 sampling points were selected in each period of excitation voltages and applied sequentially to the outer surface of PZTs. The total number of excitation cycles is 400, which can meet the steady-state time requirement of a piezoelectric vibrator. To make simulation results closer to real values, nodal voltages were coupled before solving. In addition, Beta damping is closely related to the frequency of excitation voltages. When Beta damping is not set in harmonic response analysis, the particle displacement obtained from the transient analysis does not tend to stabilize over time. After multiple attempts, it was found that when Beta damping is added, the particle displacement obtained from transient analysis tends to stabilize, which is more consistent with the actual operating states of the vibrator. Therefore, to comprehensively consider the effects on L_1, B_2, and B_4 modes, ω_i corresponding to Beta damping is defined as follows

$$\omega_i = 2\pi \frac{f_1 + f_2}{2} \tag{2}$$

where f_1 and f_2 represent the resonant frequencies of L_1 (B_2) and B_4 modes, respectively.

Fig. 6 shows the time-varying trends of the horizontal and vertical displacements of the selected point under excitation scheme 1. The response displacement of the point increases initially with time and then tends to stabilize. Fig. 7 illustrates the displacement trend of the driving point as it reaches stability.

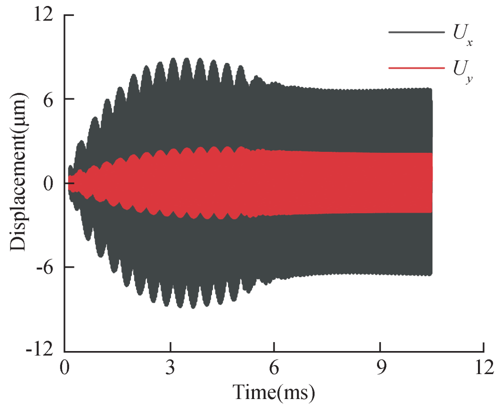

Fig.6 Displacement change curve of the selected point under excitation way 1

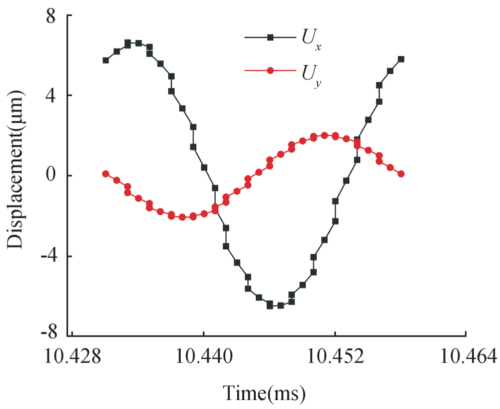

Fig.7 Stable displacement curve of the driving point under excitation way 1

When the vibration displacement of the point reaches stable, five motion cycles are selected, and the three-dimensional motion trajectory and its projection onto the XY plane are shown in Fig. 8. Although the three-dimensional motion trajectory of the point is distorted, its projection onto the XY plane is still approximately a regular ellipse, which is consistent with traditional piezoelectric motors. The distortion of the three-dimensional motion trajectory is mainly caused by the variation trend of its displacement in the z direction, which is different from the gradually stabilizing trend shown in Fig. 6. However, due to the combined action of L_1, B_2, and B_4 modes of the piezoelectric vibrator, theoretically, only in-plane vibration displacement will be generated, and the vibration displacement in the z direction can be approximately neglected. Therefore, the influence of vibration displacement of the point in the z direction on its motion trajectory is relatively small.

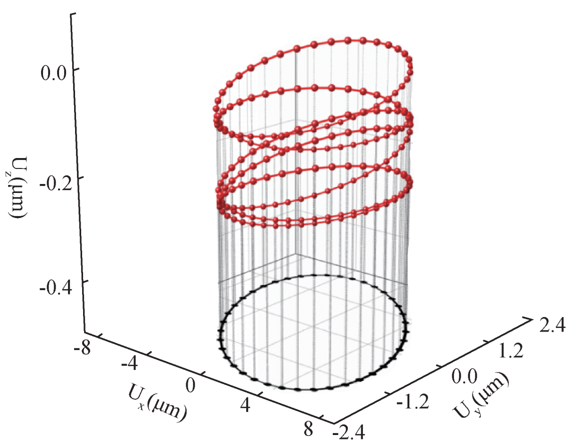

Fig.8 Motion trajectory of the point under excitation 1

To specifically investigate the influence of the addition of B_4 mode on response displacements of the point, steady-state displacements of the point was also calculated when only L_1 and B_2 modes were excited under a single-frequency excitation of 38.2 kHz. Table 3 compares steady-state displacement values of the selected point under single-frequency and dual-frequency excitation for three excitation schemes. Here, dual-frequency excitation refers to applying the resonant frequencies corresponding to B_2 (L_1) and B_4 modes to PZTs bonded to the upper and lower surfaces of the metal body, respectively, in which case modes L_1, B_2, and B_4 modes can all be excited. Single-frequency excitation refers to applying the resonant frequency of B_2 (L_1) mode to PZTs bonded to the upper and lower surfaces of the metal body, in which case only L_1 and B_2 modes can be excited. Similar to excitation scheme 1, the three-dimensional motion trajectories of the point under excitation schemes 2 and 3 also exhibit distortion, but their projections onto the XY plane remain regular ellipses. Additionally, there is little difference in steady-state displacements of the point between excitation ways 2 and 3, which is consistent with the results in Table 2 and indicates the excitation suppression of B_4 mode.

Table 3 Transient stable displacement of the point under three excitation methods

	Dual-frequency excitation (μm)		Single-frequency excitation (μm)	
	U_x	U_y	U_x	U_y
Excitation 1	6.7	2.1	5.8	1.5
Excitation 2	4.7	3.1	6.7	3.1
Excitation 3	4.7	3	7.8	4.6

By comparing the calculated results in Table 3, it can also be concluded that when only L_1 and B_2 modes are excited, response displacements of the selected point increase sequentially from excitation scheme 1 to 3, because excitation scheme 3 is more consistent with the modal shape of B_2. In addition, the addition of B_4 mode can adjust the ratio of horizontal and vertical displacements of piezoelectric vibrators. The vertical displacement of the point is larger under excitation schemes 2 and 3. The main reason may be that due to the suppression of B_4 mode, the longitudinal displacement generated by B_2 mode is relatively larger.

Furthermore, only under excitation scheme 1, steady-state response displacements of the point under dual-frequency excitation are better than that under single-frequency excitation. Therefore, under excitation scheme 1, the vibration performance of the point under dual-frequency excitation is relatively better. It not only facilitates the excitation of B_4 mode, but also allows the ratio of horizontal and vertical displacements of the point to be controlled by adjusting the amplitude of excitation voltages corresponding to the frequency of B_4 mode, thus improving the motion trajectory. At the same time, the addition of B_4 mode also broadens the frequency adjustment range of piezoelectric vibrator.

4 Modal Interaction Analysis

In reality, under L_1 mode, the chosen point of the piezoelectric vibrator primarily generates displacement in the x-direction. Under B_2 and B_4 modes, the point primarily generates displacement in the y-direction. Therefore, when L_1, B_2, and B_4 modes are simultaneously excited, response displacements of the piezoelectric vibrator can be expressed as

$$u_x = U_x \sin\left(\omega_1 t + \varphi_1\right) \tag{3}$$

$$u_y = U_{y1} \cos\left(\omega_1 t + \varphi_2\right) + U_{y2} \cos\left(\omega_2 t + \varphi_3\right) \tag{4}$$

where ω_1 and ω_2 correspond to the resonant angular frequencies of B_2 (L_1) and B_4 modes, respectively.

When a piezoelectric vibrator vibrates in B_2 or B_4 mode, it generates a simple harmonic motion with a cosine variation. When two simple harmonic motions with different frequencies (B_2 and B_4 modes) are superimposed, the trajectory of composite motion u_y is irregular but still exhibits peaks and valleys like a simple harmonic motion. Since the frequency ratio of the two modes is approximately 2, and the longitudinal displacement U_{y1} under B_2 mode is much larger than the longitudinal displacement U_{y2} under B_4 mode, the composite vibration of the point eventually tends to be stable and has little effect on the projection of the three-dimensional motion trajectory onto the XY plane. In addition, L_1, B_2, and B_4 modes actually produce a small amount of displacement in the z direction, which causes the displacement in the z direction not tend to be stable as ideally expected.

Furthermore, considering the motion curve, assuming that the phase difference between the first-order longitudinal vibration and second-order bending vibration is 90 degrees, and φ_1 is zero, then φ_2 is 90 degrees. For the sake of simplicity, assume that φ_3 is also 90 degrees. Combining formulas 2 and 3, the motion trajectory of the point can be deduced as

$$\frac{u_x^2}{U_x^2} + \frac{\left(u_y + U_{y2}\right)^2}{U_{y1}^2} = 1 + \frac{4U_{y2}}{U_{y1}} \cos^3 \omega_1 t + \frac{4U_{y2}^2}{U_{y1}^2} \cos^4 \omega_1 t \tag{5}$$

If we neglect the influence of higher-order terms in the above equation, the motion trajectory of the point remains a regular ellipse, and can be adjusted by adjusting the value of U_{y2}, which is consistent with simulation analysis. Therefore, for rectangular plate piezoelectric vibrators, multi-mode excitation actually provides a new way to adjust the motion trajectory of stator particles and broadens the frequency adjustment range of the piezoelectric vibrator.

5 Conclusion

This paper takes a rectangular plate piezoelectric vibrator as an example to analyze interactions between different vibration modes. Based on the selection criteria for operating modes of piezoelectric motors, three types of in-plane vibration modes, namely L_1, B_2, and B_4 modes, were selected. Firstly, the structure of the piezoelectric vibrator was designed according to the operating modes, and their excitation ways were also discussed. Then, the resonant frequencies of working modes were acquired by using the finite element software ANSYS. Stable displacements of the chosen driving point under harmonic response and transient analyses were all calculated. To specifically study the influence of B_4 mode on response displacements of the driving point, its steady-state displacements with and without B_4 mode were calculated and compared. Meanwhile, the motion trajectory of the point was also obtained. Finally, according to simulation results, interactions between different modes were discussed from a theoretical perspective, which contributes to the research and development of multi-mode piezoelectric motors. Moreover, under dual-frequency excitation scheme 1, the response displacements of the driving point are relatively larger. This driving way not only enhances the excitation of B_4 mode but also allows for control over the ratio of horizontal to vertical displacements. Meanwhile, the frequency adjustment range of piezoelectric vibrators is also broadened by adding B_4 mode.

Author Contribution:

Conceptualization, Funding acquisition & Writing - review: Chong Li; Writing - review & editing: Cun-yue Lu.

Foundation Information:

This research was funded by National Natural Science Foundation of China, grant number 52205292.

Data Availability:

The authors declare that the main data supporting the findings of this study are available within the paper and its Supplementary Information files.

Conflicts of Interest:

The authors declare no competing interests.

Dates:

Received 5 August 2024; Accepted 28 December 2024; Published online 31 March 2025

References

[1] S. Mukhopadhyay, B. Behera, J. Kumar. (**2021**). A brief review on the recent evolution in piezoelectric linear ultrasonic motors[J]. *Engineering Research Express* , 3(4): 042003. doi: 10.1088/2631-8695/ac3b73

[2] C. S. Zhao. (**2007**). Ultrasound motor technology and application. Science Press. 978-7-03-029048-9

[3] D. M. Xu, B. J. Zhang, S. M. Yu, et al. (**2023**). Review on single-phase driven ultrasonic motors[J]. *Journal of Intelligent Material Systems and Structures* , 34(5): 525-535. doi: 10.1177/1045389X221121911.

[4] S. Naz, T. B. Xu. (**2024**). A Comprehensive Review of Piezoelectric Ultrasonic Motors: Classifications, Characterization, Fabrication, Applications, and Future Challenges[J]. *Micromachines* , 15(9): 1170. doi: 10.3390/mi15091170.

[5] X. Zhou, S. Wu, X. Wang, et al. (**2024**). Review on piezoelectric actuators: materials, classifications, applications, and recent trends[J]. *Frontiers of Mechanical Engineering* , 19 (1): 6. doi: 10.1007/s11465-023-0772-0.

[6] L. Šišovas, A. Čeponis, S. Borodinas. (**2024**). The Challenges of Piezoelectric Actuators and Motors Application in a Space Environment[J]. *Actuators*, 13(8): 312. doi: 10.3390/act13080312.

[7] Z. Liu, Q. W. Fu, P. Yang, et al. (**2023**). Design and performance evaluation of a miniature I-shaped linear ultrasonic motor with two vibrators[J]. *Ultrasonics* , 131: 106965. doi: 10.1016/j.ultras.2023.106965.

[8] Q. S. Pan, Y. Wang, A. Wan, et al. (**2023**). Development of a novel single-mode miniature standing wave ultrasonic motor [J]. *Smart Materials and Structures* , 32(12): 125015. doi: 10.1088/1361-665X/ad07a2.

[9] X. Y. Zhou, S. Wu, X. X. Wang, et al. (**2024**) Review on piezoelectric actuators: materials, classifications, applications, and recent trends[J]. *Frontiers of Mechanical Engineering* , 19 (1): 6. doi: 10.1007/s11465-023-0772-0.

[10] C.C. Li, M. Yang, S.Y. Li. (**2009**). The excitation of vibrating shape of ultrasonic motor vibrators[J]. *Journal of Vibration and Shock* , **2009**, 28(9): 5. doi: 10.3969/j. issn. 1000-3835.2009.09.038.

[11] J. Wu, L.P. Wang, F.X. Du, et al. (**2023**) A two-DOF linear ultrasonic motor utilizing the actuating approach of longitudinal-traveling-wave/bending-standing-wave hybrid excitation[J]. *International Journal of Mechanical Sciences* , 248: 108223. doi: 10.1016/j.ijmecsci.**2023**.108223

[12] W. P. Bi, P. Q. Fan, Y. S. Wang. (**2023**). A miniature longitudinal-bending hybrid linear ultrasonic motor inspired by the planar hinged five bar mechanism[J]. *Review of Scientific Instruments* , 94(5): 055003. doi: 10.1063/5.0149155.

[13] C. Li, R.M. Chen. (**2023**) Research on interactions between different operating modes of piezoelectric motors[J]. *Smart Materials and Structures* , 32(11): 115016. doi: 10.1088/1361-665X/acfde2.